



THE UNIVERSITY *of* EDINBURGH

Edinburgh Research Explorer

A Porous Carbon with Excellent Gas Storage Properties from Recycled Polystyrene

Citation for published version:

Gatti, G, Errahali, M, Tei, L, Mangano, E, Brandani, S, Cossi, M & Marchese, L 2019, 'A Porous Carbon with Excellent Gas Storage Properties from Recycled Polystyrene', *Nanomaterials*, vol. 9, no. 5.
<https://doi.org/10.3390/nano9050726>

Digital Object Identifier (DOI):

[10.3390/nano9050726](https://doi.org/10.3390/nano9050726)

Link:

[Link to publication record in Edinburgh Research Explorer](#)

Document Version:

Peer reviewed version

Published In:

Nanomaterials

General rights

Copyright for the publications made accessible via the Edinburgh Research Explorer is retained by the author(s) and / or other copyright owners and it is a condition of accessing these publications that users recognise and abide by the legal requirements associated with these rights.


Take down policy

The University of Edinburgh has made every reasonable effort to ensure that Edinburgh Research Explorer content complies with UK legislation. If you believe that the public display of this file breaches copyright please contact openaccess@ed.ac.uk providing details, and we will remove access to the work immediately and investigate your claim.



Article

A Porous Carbon with Excellent Gas Storage Properties from Waste Polystyrene.

Giorgio Gatti ¹ , Mina Errahali ¹, Lorenzo Tei ¹, Enzo Mangano ², Stefano Brandani ², Maurizio Cossi ¹ and Leonardo Marchese ¹

¹ Dipartimento di Scienze e Innovazione Tecnologica (DISIT), Università del Piemonte Orientale, via T. Michel 11, I-15121, Alessandria, Italy; e-mail: giorgio.gatti@uniupo.it

² School of Engineering, University of Edinburgh, Sanderson Building, R. Stevenson Road, Edinburgh, UK

* Correspondence: giorgio.gatti@uniupo.it

Version April 30, 2019 submitted to *Nanomaterials*

Abstract: We describe the synthesis and the gas adsorption properties of a porous carbonaceous material, obtained from commercial expanded polystyrene. The first step consists in the Friedel-Craft reaction of the dissolved polystyrene chains with a bridging agent, to form a highly-crosslinked polymer, with permanent porosity of 0.7 cm³/g; then this polymer is treated with potassium hydroxide at high temperature to produce a carbon material with porous volume larger than 1.4 cm³/g and a distribution of ultramicro-, micro- and mesopores. After characterization of the porous carbon and determination of the bulk density, the methane uptake was measured using a volumetric apparatus to pressures up to 30 bar. The equilibrium adsorption isotherm obtained is among the highest ever reported for this kind of materials. The interest of this product lies both in its excellent performance and in the virtually costless starting material.

Keywords: porous carbon; hyper-crosslinked polymer; methane storage; waste valorization

1. Introduction

The numerous applications of methane as energy vector would benefit greatly from adsorbed natural gas (ANG) technologies, [1–3] which are expected to compensate the relatively low energy density of gaseous methane reducing the costs related to compressed or liquified natural gas (CNG or LNG, respectively) approaches. With suitable adsorbers the gas storage pressure in tanks could be lowered up to 20% of the value necessary in CNG,[4] or alternatively the stored quantity could be largely increased at the same pressure. These expectations have been quantified by the U.S. Department of Energy (DOE) with the storage target of 180 cm³(STP)/cm³ at 35 bar, raised successively to 263 cm³(STP)/cm³, a value judged too ambitious by some researchers, however.[5]

Among the various classes of materials proposed for ANG applications, [6–15] activated porous carbons seem the most promising for several reasons: [3,4,16–21] versatility, which allows to tune the porosity by tailoring the starting materials and the reaction conditions, high mechanical and chemical stability, and not leastly the possibility to design cheap and scalable productions.

Here we describe the preparation and the characterization of a porous carbon with a very high methane uptake capacity, obtained through an easy and scalable reaction from expanded polystyrene (a virtually costless material which can be recycled from the packaging industry). The very good performances of this adsorber are related to the favorable pore distribution in the regions of micropores (7 – 20 Å) and small mesopores (20 – 50 Å) coupled to high bulk density, leading to an unusually large uptake on a volume basis.

The material was prepared in two steps: first, a hyper-crosslinked (HPC) polymer was obtained with Friedel-Crafts reaction from expanded polystyrene (PS): this material is referred to as HPC-PS

33 in the following. HPC polymers are widely studied[22–28] for their simplicity of synthesis[29–31]
34 and excellent mechanical and textural properties. Cooper *et al.* studied the crosslinking reaction
35 of various polystyrenes synthesized in situ with different molecular weights;[32] Fu *et al.* reported
36 the same reaction on expanded PS, using 1,2-dichloroethane as crosslinking agent.[33] Very recently,
37 waste polystyrene foam was used to prepare cross-linked polymers through Friedel-Crafts reaction
38 with acetone and aluminum chloride in the presence of silica nanoparticles, followed by calcination to
39 obtain a porous carbon;[34] another porous carbon was prepared from PS by pyrolysis and chemical
40 activation with KOH.[35] Then HPC-PS was chemically and thermally activated, producing a highly
41 porous carbonaceous material, named KPS-1. Analogous procedures were employed recently to
42 prepare porous carbons from HCP:[36–40] we also have followed this approach in the past starting
43 from tetraphenylmethane, testing different reaction conditions to optimize the textural properties of
44 the products.[31,41,42]

45 2. Materials and Methods

46 As mentioned above[31,32] and illustrated in Figure 1, the hyper-crosslinked polymer HPC-PS
47 was obtained with Friedel-Crafts reaction from expanded polystyrene (PS), using ferric chloride
48 as catalyst and formaldehyde dimethyl acetal (FDA) as bridging agent. 20 g of polystyrene from
49 packaging (PS) and 93.1 g of FeCl_3 (0.57 mol) were suspended in 0.54 L of dichloroethane (DCE). The
50 mixture was stirred mechanically at room temperature to obtain a homogeneous solution; then 54 mL
51 (0.61 mol) of formaldehyde dimethylacetal (FDA) were added dropwise. The mixture was stirred at
52 RT for 30 min and then heated at 80 °C for 18 h. After cooling to room temperature, the thick gel was
53 diluted with ethanol and washed several times with EtOH and water until neutral pH was reached.
54 Finally, the solid was dried in the oven at 110 °C overnight (the material obtained is named HPC-PS).

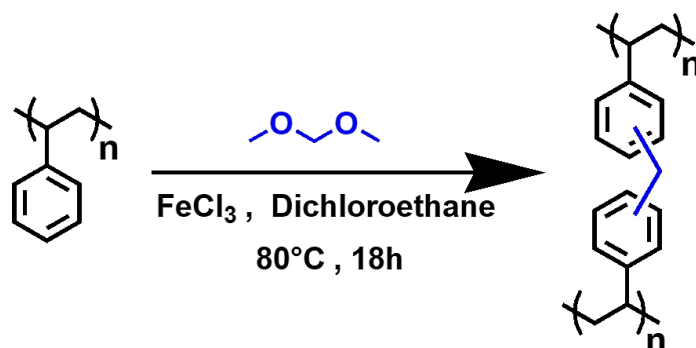


Figure 1. Formation of hyper-crosslinked polymeric material, HPC-PS, from polystyrene with Friedel-Crafts reaction using FDA as linker.

55 To obtain the porous carbon, 2 g of HPC-PS were homogeneously grinded with 6 g of KOH
56 (0.107 mol) under inert conditions. Then, the mixture was placed in a crucible of alumina and
57 thermally treated under N_2 flow with a ramp of 2 °C / min up to 800 °C and subsequently held
58 under isothermal conditions for 1h. After the chemical activation,[23] all the resulting carbons were
59 washed with deionized water (250 mL), with 2M HCl (200 mL) and washed again with deionized
60 water to remove potassium salts and to neutralize the solution, and then dried at 110 °C for 18 hours
61 (the final material is named KPS-1).

62 The materials were characterized by FTIR spectra, recorded with a Bruker Equinox 55
63 spectrometer, equipped with a DTGS pyroelectric detector with 4 cm^{-1} resolution, and Raman
64 spectra, recorded on as prepared powders using a Jobin Yvon HR800 Lab-Ram μ -spectrometer,
65 equipped with an Olympus BX41 microscope, a He-Ne 20 mW laser working at 632.8 nm, and a
66 charge-coupled device (CCD).

67 The pore structures of HPC-PS and KPS-1 were investigated by adsorbing N₂ at 77 K and CO₂
68 at 273 K and analyzing the adsorption isotherms with Quenched Solid Density Functional Theory
69 (QSDFT) method (using carbon slit/cylindrical pore parameters).[43,44]

70 Solid-state NMR spectra were acquired on a Bruker Avance III 500 spectrometer and a wide
71 bore 11.7 Tesla magnet with operational frequencies for ¹H and ¹³C of 500.13 and 125.77 MHz,
72 respectively. A 2.5 mm double resonance probe with MAS was employed in all experiments. The
73 magnitude of radio frequency field was 131 kHz for ¹H MAS NMR and relaxation delays, d1, between
74 accumulations was 3 s. For the ¹³C cross-polarization (CP) magic angle spinning (MAS) experiments,
75 the proton radio frequency (RF) of 100 and 42 kHz were used for initial excitation and decoupling,
76 respectively.

77 During the CP period the ¹H RF field was ramped using 100 increments, whereas the ¹³C RF
78 field was maintained at a constant level. During the acquisition, the protons were decoupled from
79 the carbons by using a Spinal64 decoupling scheme. A moderate ramped RF field of 54 kHz was used
80 for spin locking, while the carbon RF field was matched to obtain optimal signal and CP contact times
81 of 0.5 ms were used. The ¹³C NMR spectra were also acquired using DP (direct polarization) MAS
82 based experiments under high power proton decoupling conditions.

83 To avoid baseline distortions and to remove ¹³C background signals associated with the probe
84 in DPMAS experiments, special pulse program (aringdec) was used from the Bruker topspin library.
85 The magnitude of radio frequency field was 80 kHz for ¹³C MAS NMR and the ¹H decoupling field
86 was 66 kHz as well as the relaxation delays, d1, between accumulations was 30 s. All chemical shifts
87 are reported using δ scale and are externally referenced to TMS at 0 ppm.

88 3. Results and Discussion

89 3.1. Vibrational Characterization

90 The FTIR spectrum of HPC-PS is reported in Figure 2. In the high frequency region, both the
91 PS precursor (curve a) and the HCP polymer (curve b) are characterized by bands at 3100-3000 cm⁻¹,
92 attributed to aromatic C-H groups stretching modes. After polymerization the group of bands in the
93 region 3000-2800 cm⁻¹ due to the stretching of aliphatic C-H, became more intense due to methylene
94 linkers between the aromatic rings. The low frequency region shows in the PS spectrum the structural
95 bands due to -CH₂ and aromatic -CH₂ bending bands. The spectrum of HCP polymer shows
96 new bands in the region 1800-1700 cm⁻¹ and 950-650 cm⁻¹ due to the higher number of positions
97 substituted on the aromatic rings after the polymerization. Also the bands at 1450 cm⁻¹ due to -CH₂
98 bending mode of the methylene linker along with the band 1262 cm⁻¹ due to -CH₂ wagging modes
99 of the chloro-methylene groups, confirm the successful cross-linking reaction.

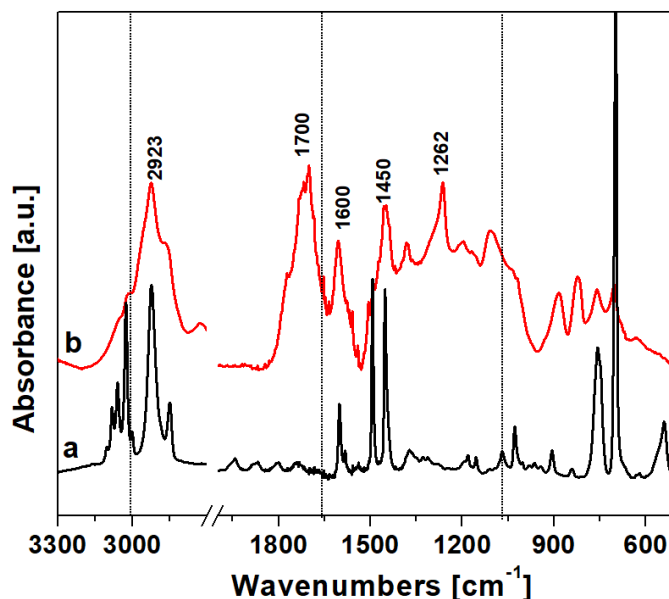


Figure 2. FTIR spectra in the region $3300\text{--}500\text{ cm}^{-1}$ of HCP polymer (a) and PS precursor (b).

100 Raman spectroscopy was used to evaluate the carbonization degree after the KOH-activated
 101 thermal process described above: the spectrum of KPS-1 is shown in Figure 3. KPS-1 Raman spectrum
 102 shows two main vibrational modes at 1329 cm^{-1} and 1593 cm^{-1} . The 1593 cm^{-1} mode (G peak)
 103 corresponds to the Raman-allowed E_{2g} mode in the ideal graphite, and the 1329 cm^{-1} mode (D
 104 peak) corresponds to the disorder-induced band, which is associated to the large density of phonon
 105 states.[45] In particular, the strong D-band peak demonstrates that the microporous carbon has a low
 106 degree of graphitization ($I_D/I_G = 1.16$) and contains a significant amount of disordered sections and
 107 defects.[46]

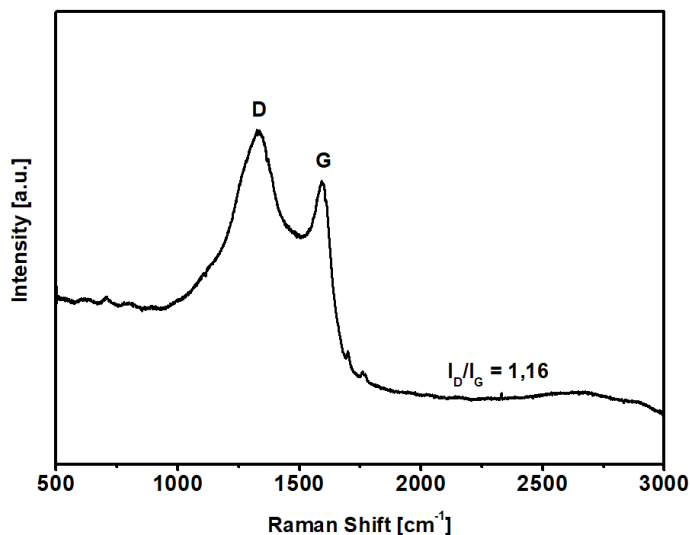


Figure 3. Raman spectrum of KPS-1 carbon sample in the region $3000\text{--}500\text{ cm}^{-1}$.

108 3.2. Pore Size Analysis

109 To evaluate the textural properties of the synthesized materials, we measured the adsorption
 110 isotherms of nitrogen at 77 K and carbon dioxide at 293 K both in HPC-PS and in KPS-1. With
 111 N_2 , HCP-PS shows a type IV isotherm (with BET specific surface area, SSA_{BET} , of $739\text{ m}^2/\text{g}$) with
 112 a pronounced hysteresis loop between 0.9 and about 0.4 P/P_0 , evidencing the presence of mesopores

113 in the material. On the other hand, the derivated carbon KPS-1 shows a pseudo Langmuir isotherm
 114 of type I ($SSA_{BET} = 2637\text{m}^2/\text{g}$) and a small hysteresis loop of type H4 that can be associated to the
 115 presence of narrow slit pores, as commonly found for nitrogen sorption isotherm on activated carbons.
 116 The porosity of both the materials was described in greater detail by applying QSDFT analysis to the
 117 adsorption isotherms.

118 The N_2 adsorption isotherms for the two materials are shown in Figure 4, and the corresponding
 119 pore size distributions (PSD) and cumulative pore volumes (CPV) are compared in Figure 5.

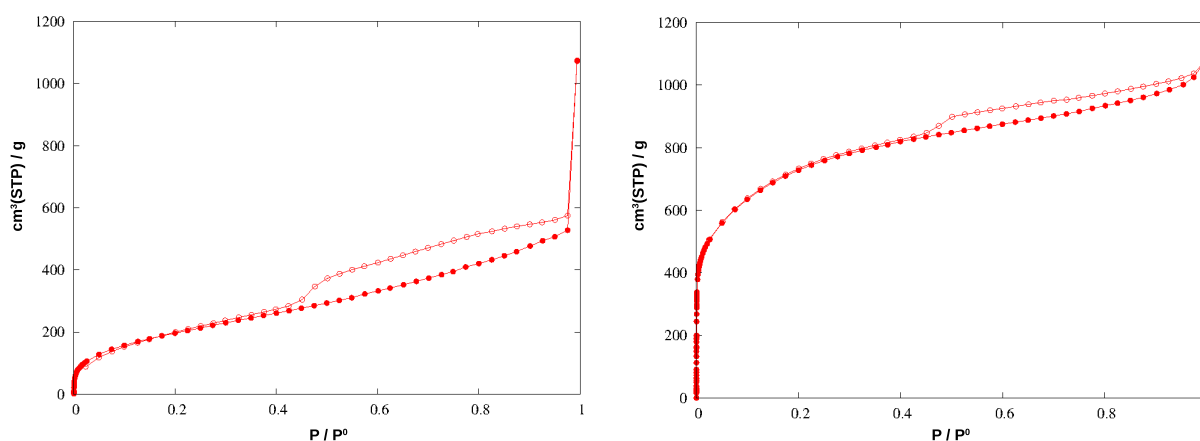


Figure 4. Adsorption (filled circles) and desorption (empty circles) isotherms of N_2 at 77 K in HPC-PS (left) and KPS-1 (right).

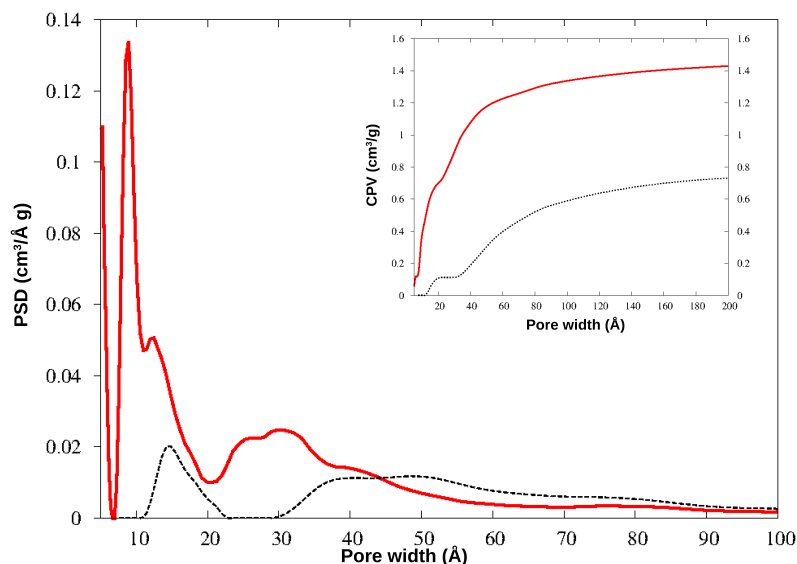


Figure 5. Pore size distribution (PSD) and cumulative pore volume (CPV) for HPC-PS (black dotted line) and KPS-1 (red solid line) from N_2 adsorption at 77 K.

120 In KPS-1 a rich family of micropores appears below 10Å : to investigate this region in greater
 121 detail, this material was further analyzed by adsorbing CO_2 at 273 K: the QSDFT analysis was applied
 122 to the CO_2 isotherm, providing the PSD and CPV for ultramicropores, reported in Figure 6. The
 123 smallest pores are described in much greater detail by CO_2 adsorption at the higher temperature, as
 124 well known: the ultramicropores around $4\text{-}7\text{Å}$ width are clearly characterized by this experiment.
 125 Notably both gases find a family of micropores at 9Å , though their relative abundance is different

126 in N₂ and CO₂ curves: however, the two gases provide very similar values for the total microporous
 127 volume (CPV).

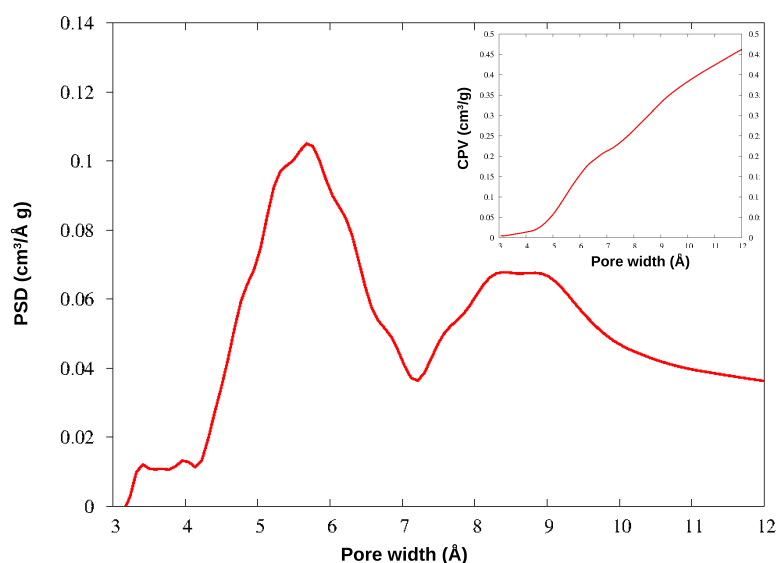


Figure 6. PSD and CPV for KPS-1 from CO₂ adsorption at 273 K.

128 The HPC polymer presents a porous volume of 0.74 cm³/g, of which 0.11 cm³/g due to
 129 micropores (below 20 Å width): the analogous systems prepared by Friedel-Crafts reaction from
 130 tetraphenylmethane, in different conditions, showed porous volumes in the range 0.64 – 0.83 cm³/g,
 131 with microporous contributions from 0.16 to 0.21 cm³/g.[31] Other HPC polymers obtained from
 132 benzene, thiophene and pyrrole were found to have porous volumes of 1.52 (0.40), 0.33 (0.22) and
 133 0.25 (0.14) cm³/g, respectively (in parentheses the microporous volumes).[16]

134 After the chemical and thermal activation, the porosity increases significantly, exceeding 1.40
 135 cm³/g (note that pores above 200 Å width, approximately, become less and less important in gas
 136 adsorption processes), and the pore distribution changes deeply too. The same effect was reported
 137 after the carbonization of the HPC polymers mentioned above: their porous volume increased to 1.58
 138 (for benzene monomer), 1.51 (thiophene) and 3.14 (pyrrole) cm³/g.[16]

139 The micropores in HPC-PS appear in a quite narrow distribution around 15 Å, while the
 140 mesopore family is widely spread above 30 Å width. In KPS-1, on the other hand, micropores split in
 141 two narrow peaks around 9 and 13 Å, and ultramicropores appear also, between 5 and 6 Å, as clearly
 142 shown by CO₂ PSD in Figure 6. Overall the KPS-1 microporous volume reaches 0.7 cm³/g; a large
 143 family of mesopores appears between 20 and 40 Å, adding 0.4 cm³/g to the porous volume, while a
 144 broad distribution of mesopores exist with larger size, contributing with 0.32 cm³/g, approximately,
 145 to the total volume. The porous volumes of the materials are resumed in Table 1, and compared to
 146 the volumes recently reported for other porous carbons obtained from PS.

147 3.3. SS-NMR

148 The nature of hyper-crosslinking in HPC-PS was also investigated using solid-state ¹³C and ¹H
 149 NMR spectroscopy: HPC-PS ¹³C CPMAS NMR spectrum, recorded using 0.5 ms cross polarization
 150 contact time and 20 kHz MAS rate, is shown in Figure 7.

Material	Total	Microporous	Mesoporous
HPC-PS	0.74	0.11	0.63
KPS-1	1.42	0.70	0.72
PC from ref. [34]	0.7	-	0.7
AC800 from ref. [35]	1.20	0.93	0.27

Table 1. Porous volume (cm^3/g) of the produced materials.

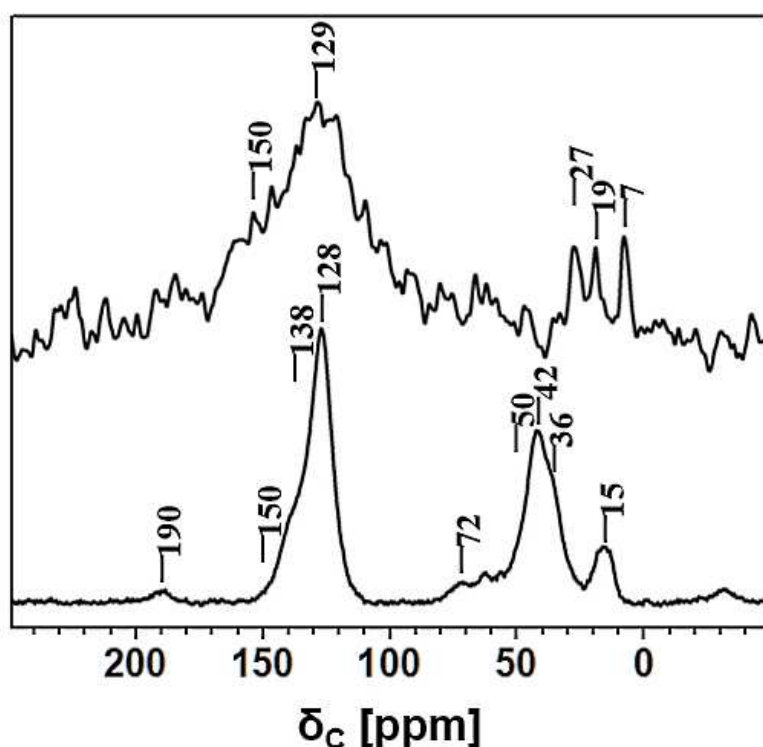


Figure 7. ^{13}C NMR spectra: (a) HPC-PS recorded using CPMAS technique with CP contact time of 0.5 ms; (b) KPS-1 recorded using DPMAS technique with a MAS rate of 30 kHz.

151 Aromatic ^{13}C peaks in the range 120-150 ppm are assigned as following: 128 ppm for the
 152 aromatic C-H and 138 ppm for the methylene- and/or methine-substituted aromatic carbons;[31,47]
 153 there are no ^{13}C resonances above 145 ppm confirming the absence of free polystyrene units in
 154 HPC-PS[48].

155 In the aliphatic region, the ^{13}C resonances at 42 and 36 ppm are assigned to the methylene
 156 units of the polystyrene blocks and to the CH_2 (benzylic carbon) linker. Polystyrene methine carbons
 157 appeared as a very broad resonance centered at 50 ppm and this assignment was further supported
 158 by the intensity increase in long contact-time CPMAS experiment (data not shown). Additional
 159 resonance, at 72 ppm, is assigned to CH_2OH groups, substituted on the aromatic rings.[31] On the
 160 other hand, CH_2Cl carbons formed in the benzene chloromethylation during Friedel-Crafts reaction
 161 are expected at 43 ppm and their presence cannot be ruled out. Moreover, a strong broad peak is
 162 also observed at 15 ppm and assigned to a CH_3 group due to the methylation and/or ethylation of
 163 aromatic rings;[49] the unusual broad peak observed at around 190 ppm is tentatively assigned to
 164 carbonyl carbons.

165 Likewise, ^{13}C NMR spectrum is recorded on carbonized material, KPS-1: in this case, we
166 employed ^{13}C DPMAS (direct polarization magic angle spinning) NMR technique, since the low
167 proton content and the influence of paramagnetic interactions in KPS-1 are problematic for recording
168 a ^{13}C NMR spectrum using CPMAS technique.[50]

169 Indeed, a combination of several technical challenges such as highly electric conductive nature
170 of carbonized material, magnetic susceptibility effects as observed in graphitic material, very low
171 isotopic abundance of ^{13}C , very long carbon recycle delay and the low sample volume (less than 10
172 mg in a 2.5 mm rotor) made the acquisition of a good ^{13}C spectrum quite problematic.[50]

173 Nevertheless, the ^{13}C spectrum of KPS-1, obtained at MAS rate of 30 kHz and shown in Figure 8,
174 revealed a very broad resonance in the aromatic region and three narrow resonances in the aliphatic
175 region. A typical resonance of a carbonized material appears at 129 ppm with a down-field shoulder
176 at 150 ppm. The broad peak centered at 129 ppm is assigned to the presence of sp^2 hybridized carbons
177 sites as in graphitic material[51–54] Furthermore, the broad shoulder centered at 150 ppm is due to the
178 advancement of polycyclization of the benzene rings during carbonization. The narrow resonances
179 at 7, 19 and 27 ppm are either due to the methyl and ethyl carbons generated upon the methylene
180 disproportionation during carbonization and/or due to the entrapped aliphatic carbon fragments in
181 the hierarchical pores of the material.

182 To further test the above hypothesis, we have employed ^1H MAS NMR technique, which
183 proved particularly useful for studying molecular adsorption inside porous carbon materials. As
184 shown in Figure 8, HPC-PS polymeric material presents peaks due to both aliphatic and aromatic
185 protons. Upon carbonization of the hyper-crosslinked polymeric material, intensity due to aromatic
186 and aliphatic protons decreases dramatically and intense multiple resonances appear at around -3
187 ppm (Figure 8 and inset).

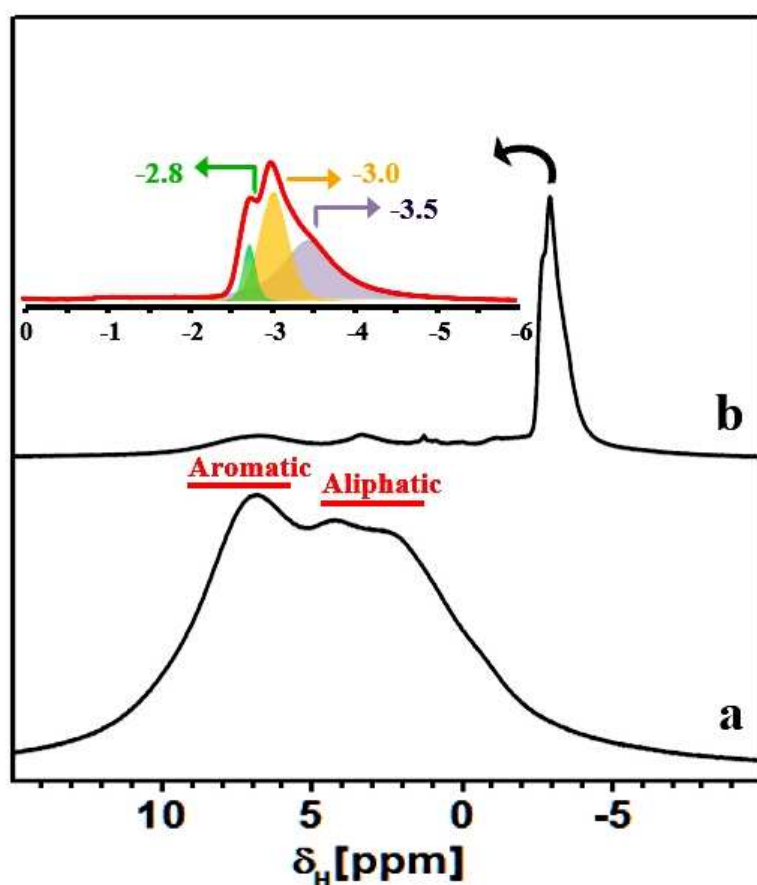


Figure 8. ^1H MAS NMR spectra of HPC-PS (a) and KPS-1 (b) recorded using a MAS rate of 15 kHz. Inset: zoomed KPS-1 spectrum.

Such a strong up-field ^1H shift (relative to TMS at 0 ppm) is highly unusual for aliphatic protons: however, proton species close to porous carbon surfaces can experience a reduced local magnetic field owing to the circulation of nearby delocalized π -electrons leading to large chemically-shielded proton environments. The protonic species can be either structural or adsorbed in nature and their chemical shifts can be influenced by the carbon ring currents as has been reported for plane and curved graphene sheets, nanotubes and fullerene like elements[55–57]. As discussed above, these protonic species are probably associated with the aliphatic carbons fragments that appeared in the ^{13}C NMR spectrum. However, a further NMR characterization is necessary for the detailing of chemical compositions of KPS-1 and is beyond the scope of this communication.

Then ^{13}C and ^1H NMR spectroscopy has unambiguously confirmed the hyper-crosslinking of the polystyrene units during the formation of HPC-PS. Moreover, carbon linkages as benzylic units, derived from FDA, between aromatic rings were identified. Finally, polycyclization of the benzene rings and the aliphaticization of aromatic rings during carbonization were also determined.

3.4. Methane Adsorption

Before testing the methane adsorption in KPS-1, the synthesized fine powder has to be compressed in tablets, allowing the measure of the packing density (sometimes referred to as bulk density, too), used to estimate the volume-based gas uptake. After the compression, KPS-1 packing density was 0.50 g/cm^3 : the PSD and CPV were measured again on the compressed sample, without significant changes with respect to the as-synthesized powder up to pores of 200 \AA width, showing that packing does not affect the micro- and mesopore network, while removing the interparticle voids and possibly part of the macropores.

Material	Pressure (bar)	Mass-based uptake (g/g)	Volume-based uptake (cm ³ (STP)/cm ³)	Bulk density (g/cm ³)	ref.
KPS-1	30	0.209	146	0.50	this work
LMA738	35	0.191	142	0.53	[18]
PY100_700	35	0.178	150	0.60	[4]
DO100_700	35	0.182	160	0.62	[4]
K-PAF-1-750	35	0.207	n. a.	n. a.	[59]
KOH-corncob	35	0.25	n. a.	n. a.	[60]
Activ. monolith	30	0.136	154	0.80	[17,20]

Table 2. Excess uptake of CH₄ at 298 K in KPS-1 and in some of the best performing materials.

209 The uptake of methane on mass and volume bases, measured for compressed KPS-1 at 298 K
 210 with the procedure described in ref. [58], is shown in Figure 9, compared to the data reported in
 211 ref. [18] for one of the best performing porous carbons (LMA738), often used as benchmark for
 212 methane adsorption. Note that both volume- and mass-based uptakes are of interest for large scale
 213 applications, depending on whether the final weight or volume of the container is the limiting factor.

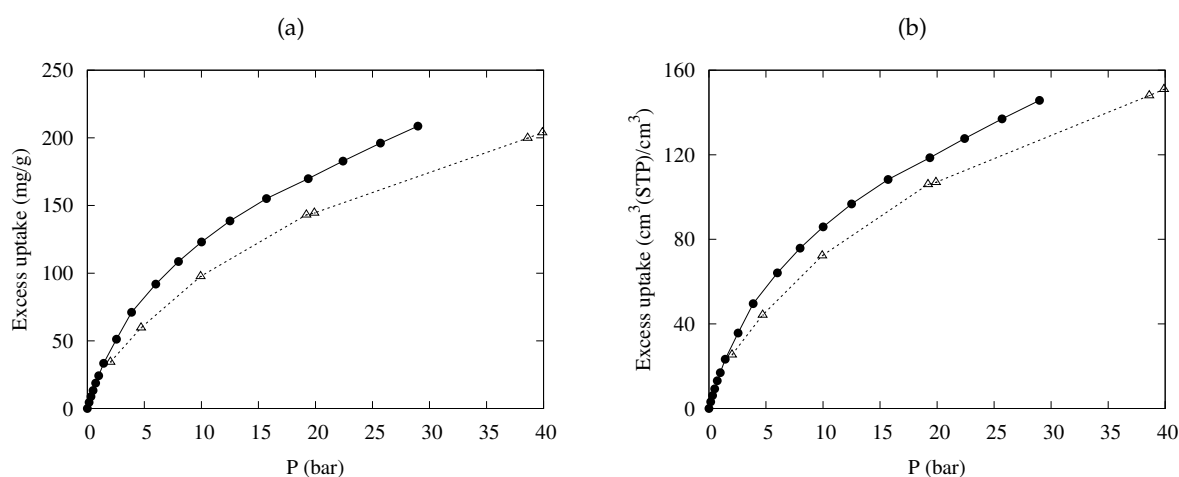


Figure 9. Excess adsorption isotherms at 298 K for CH₄ on mass basis (a) and on volume basis (b) in KPS-1 (solid circles) and LMA738 (open triangles) [18].

214 The results are very satisfying: at intermediate pressure (about 30 bar) both measures of uptake
 215 are markedly superior to the results of the best carbon-based materials described so far. The good
 216 mass-based uptake can be ascribed to the high microporosity (effective at low pressure) coupled to
 217 a large fraction of “small” mesopores (20 – 40 Å wide) but also to a long tail of wider mesopores,
 218 so that the adsorption is very high throughout the whole pressure range. Furthermore the packing
 219 density is large enough to maintain the good performance also in the volume-based scale.

220 The adsorption performance of KPS-1 is compared to the results obtained at the same
 221 temperature for the best carbon-based materials in Table 2.

Another measure of the gas uptake has been suggested recently, namely the storage capacity,[18] designed to predict more accurately the performance of a given adsorber in real operative conditions.

The storage capacity (n_{stg}), expressing the density of gas stored in an actual tank completely filled by the adsorber, is defined by the following equation:

$$n_{stg} = n_{exc} + \rho_{gas} \left(1 - \frac{\rho_{pack}}{\rho_{He}} \right) \quad (1)$$

222 combining the excess uptake on volume basis (n_{exc}) with the free gas density (ρ_{gas}): the quantity
 223 in parenthesis estimates the fraction of “dead volume” in the container from the adsorbent skeleton
 224 density (ρ_{He}) and its packing density (ρ_{pack}). KPS-1 skeleton density was measured by helium
 225 pycnometry as 2.32 g/cm³, a rather high value confirming that the material is strongly amorphous,
 226 as suggested by Raman spectra.

227 The storage density provided by KPS-1 is reported in Figure 10: also in this case KPS-1
 228 performance is extremely good, as the storage capacity reaches 168 cm³(STP)/cm³ at 30 bar, larger
 229 than the best result published so far for a porous carbon (148 cm³(STP)/cm³ for LMA738 in ref. [18]).

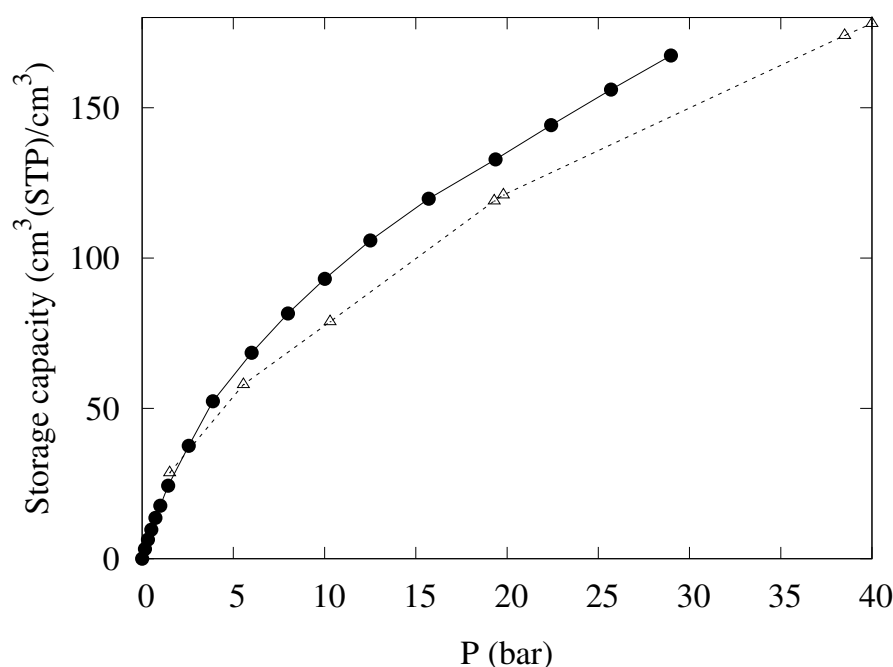


Figure 10. Storage density at 298 K for CH₄ in KPS-1 (solid circles) and LMA738 (open triangles) [18].

230 4. Conclusions

231 We have described a new porous carbon material (KPS-1) able to adsorb a very large quantity of
 232 gaseous methane in a wide range of pressures. The material was obtained first by Friedel-Crafts
 233 reaction on expanded polystyrene, to get a highly hyper-crosslinked polymer (HPC-PS), and
 234 then with an activated carbonization of this polymer. Both HPC-PS and KPS-1 were carefully
 235 characterized by FTIR and Raman spectroscopy, which showed the degree of polymerization first
 236 and of carbonization after the activation process, as well as by SS-NMR, providing details on the
 237 nature of the chemical moieties formed in the process. Then the porosity of both the polymer and the
 238 activated carbon were estimated with QSDFT analysis of nitrogen and CO₂ adsorption isotherms.

239 Thanks to the optimal combination of micro- and mesoporosity and packing density, KPS-1
 240 presented mass-based and volume-based methane uptakes, as well as storage capacities, among the
 241 highest presented so far for this kind of materials. No less important, KPS-1 was synthesized starting
 242 from a commercial expanded polystyrene peanut through a cheap and easily scalable procedure,
 243 suggesting the possibility of a large scale production from recycled materials. The KPS-1 adsorption

244 capacity towards other gases, primarily CO₂, as well as the test of various sources of expanded PS,
245 with different molecular weights of the starting material, will be described in future works.

246 **Author Contributions:** G.G. and M.E. proposed the idea; G.G., M.E. and L.T. synthesized the materials; G.G.
247 and M.E. characterized the samples; E.M. and S.B. measured the methane adsorption; M.C. and L.M. supervised
248 the work and provided funding; G.G. and M.C. wrote the paper. All the authors have discussed and critically
249 reviewed the manuscript, and agreed with all the content.

250 **Funding:** This work was funded by SOL Group and by the Italian Ministry of Education, University and
251 Research (PRIN-2010A2FSS9).

252 **Acknowledgments:** Prof. Katia Sparnacci (Università del Piemonte Orientale) is warmly thanked for the
253 measure of PS molecular weight.

254 **Conflicts of Interest:** The authors declare no conflict of interest.

255 References

- 256 1. Byamba-Ochir, N.; Shim, W.; Balathanigaimani, M.; Moon, H. High Density Mongolian Anthracite
257 Based Porous Carbon Monoliths for Methane Storage By Adsorption. *Applied Energy* **2017**, *190*, 257–265.
258 doi:10.1016/j.apenergy.2016.12.124.
- 259 2. Rash, T.; Gillespie, A.; Holbrook, B.; Hiltzik, L.; Romanos, J.; Soo, Y.; Sweany, S.; Pfeifer, P.
260 Microporous Carbon Monolith Synthesis and Production for Methane Storage. *Fuel* **2017**, *200*, 371–379.
261 doi:10.1016/j.fuel.2017.03.037.
- 262 3. Kizzie, A.; Dailly, A.; Perry, L.; Lail, M.; Lu, W.; Nelson, T.; Cai, M.; Zhou, H.C. Enhanced Methane
263 Sorption in Densified Forms of a Porous Polymer Network. *Mater. Sci. Appl.* **2014**, *5*, 387–394.
- 264 4. Casco, M.; Martínez-Escandell, M.; Kaneko, K.; Silvestre-Albero, J.; Rodríguez-Reinoso, F. Very High
265 Methane Uptake on Activated Carbons Prepared from Mesophase Pitch: a Compromise Between
266 Microporosity and Bulk Density. *Carbon* **2015**, *93*, 11–21. doi:10.1016/j.carbon.2015.05.029.
- 267 5. Simon, C.; Kim, J.; Gomez-Gualdrón, D.; Camp, J.; Chung, Y.; Martin, R.; Mercado, R.; Deem,
268 M.; Gunter, D.; Haranczyk, M.; Sholl, D.; Snurr, R.; Smit, B. The Materials Genome in Action:
269 Identifying the Performance Limits for Methane Storage. *Energy Environ. Sci.* **2015**, *8*, 1190–1199.
270 doi:10.1039/c4ee03515a.
- 271 6. Makal, T.; Li, J.R.; Lu, W.; Zhou, H.C. Methane Storage in Advanced Porous Materials. *Chem. Soc. Rev.*
272 **2012**, *41*, 7761–7779. doi:10.1039/c2cs35251f.
- 273 7. He, Y.; Zhou, W.; Yildirim, T.; Chen, B. A Series of Metal-organic Frameworks with High Methane
274 Uptake and An Empirical Equation for Predicting Methane Storage Capacity. *Energy Environ. Sci.* **2013**,
275 *6*, 2735–2744. doi:10.1039/c3ee41166d.
- 276 8. Konstas, K.; Osl, T.; Yang, Y.; Batten, M.; Burke, N.; Hill, A.; Hill, M. Methane Storage in Metal Organic
277 Frameworks. *J. Mater. Chem.* **2012**, *22*, 16698–16708. doi:10.1039/c2jm32719h.
- 278 9. Furukawa, H.; Yaghi, O. Storage of Hydrogen, Methane, and Carbon Dioxide in Highly Porous Covalent
279 Organic Frameworks for Clean Energy Applications. *J. Am. Chem. Soc.* **2009**, *131*, 8875–8883.
280 doi:10.1021/ja9015765.
- 281 10. Feng, X.; Ding, X.; Jiang, D. Covalent Organic Frameworks. *Chem. Soc. Rev.* **2012**, *41*, 6010–6022.
282 doi:10.1039/c2cs35157a.
- 283 11. Xiang, Z.; Cao, D. Porous Covalent-organic Materials: Synthesis, Clean Energy Application and Design.
284 *J. Mater. Chem. A* **2013**, *1*, 2691–2718. doi:10.1039/c2ta00063f.
- 285 12. Yuan, D.; Lu, W.; Zhao, D.; Zhou, H.C. Highly Stable Porous Polymer Networks with Exceptionally High
286 Gas-uptake Capacities. *Advanced Materials* **2011**, *23*, 3723–3725. doi:10.1002/adma.201101759.
- 287 13. Ben, T.; Pei, C.; Zhang, D.; Xu, J.; Deng, F.; Jing, X.; Qiu, S. Gas Storage in Porous Aromatic Frameworks
288 (PAFs). *Energy Environ. Sci.* **2011**, *4*, 3991–3999. doi:10.1039/c1ee01222c.
- 289 14. Wood, C.; Tan, B.; Trewin, A.; Su, F.; Rosseinsky, M.; Bradshaw, D.; Sun, Y.; Zhou, L.; Cooper,
290 A. Microporous Organic Polymers for Methane Storage. *Adv. Mater.* **2008**, *20*, 1916–1921.
291 doi:10.1002/adma.200702397.
- 292 15. Cooper, A. Conjugated Microporous Polymers. *Adv. Mater.* **2009**, *21*, 1291–1295.
293 doi:10.1002/adma.200801971.

- 294 16. Lee, S.J.; Bae, Y.S. Review of Molecular Simulations of Methane Storage in Metal-organic Frameworks. *J.*
295 *Nanosci. Nanotech.* **2016**, *16*, 4284–4290. doi:10.1166/jnn.2016.10974.
- 296 17. Marco-Lozar, J.; Kunowsky, M.; Carruthers, J.; Linares-Solano, A. Gas Storage Scale-up
297 At Room Temperature on High Density Carbon Materials. *Carbon* **2014**, *76*, 123–132.
298 doi:10.1016/j.carbon.2014.04.058.
- 299 18. Casco, M.; Martínez-Escandell, M.; Gadea-Ramos, E.; Kaneko, K.; Silvestre-Albero, J.; Rodríguez-Reinoso,
300 F. High-pressure Methane Storage in Porous Materials: Are Carbon Materials in the Pole Position? *Chem.*
301 *Mater.* **2015**, *27*, 959–964. doi:10.1021/cm5042524.
- 302 19. Alonso, A.; Moral-Vico, J.; Abo Markeb, A.; Busquets-Fité, M.; Komilis, D.; Puntès, V.; Sánchez, A.; Font,
303 X. Critical Review of Existing Nanomaterial Adsorbents to Capture Carbon Dioxide and Methane. *Sci.*
304 *Total Environ.* **2017**, *595*, 51–62. doi:10.1016/j.scitotenv.2017.03.229.
- 305 20. Marco-Lozar, J.; Kunowsky, M.; Suárez-García, F.; Carruthers, J.; Linares-Solano, A. Activated
306 Carbon Monoliths for Gas Storage At Room Temperature. *Energy Environ. Sci.* **2012**, *5*, 9833–9842.
307 doi:10.1039/c2ee22769j.
- 308 21. Marco-Lozar, J.; Juan-Juan, J.; Suárez-García, F.; Cazorla-Amorós, D.; Linares-Solano, A. MOF-5 and
309 Activated Carbons as Adsorbents for Gas Storage. *International Journal of Hydrogen Energy* **2012**,
310 *37*, 2370–2381. doi:10.1016/j.ijhydene.2011.11.023.
- 311 22. Xu, S.; Luo, Y.; Tan, B. Recent Development of Hypercrosslinked Microporous Organic Polymers.
312 *Macromol. Rapid Commun.* **2013**, *34*, 471–484. doi:10.1002/marc.201200788.
- 313 23. Li, B.; Gong, R.; Wang, W.; Huang, X.; Zhang, W.; Li, H.; Hu, C.; Tan, B. A New Strategy to Microporous
314 Polymers: Knitting Rigid Aromatic Building Blocks By External Cross-linker. *Macromolecules* **2011**,
315 *44*, 2410–2414. doi:10.1021/ma200630s.
- 316 24. Ding, L.; Gao, H.; Xie, F.; Li, W.; Bai, H.; Li, L. Porosity-Enhanced Polymers from Hyper-Cross-Linked
317 Polymer Precursors. *Macromolecules* **2017**, *50*, 956–962. doi:10.1021/acs.macromol.6b02715.
- 318 25. Davankov, V.A.; Tsyurupa, M.P. *Hypercrosslinked Polymeric Networks and Adsorbing Materials*; Vol. 56,
319 *Comprehensive Analytical Chemistry*, Elsevier, 2011.
- 320 26. Slater, A.; Cooper, A. Function-led Design of New Porous Materials. *Science* **2015**, *348*, aaa8075.
321 doi:10.1126/science.aaa8075.
- 322 27. Tan, L.; Tan, B. Hypercrosslinked Porous Polymer Materials: Design, Synthesis, and Applications. *Chem.*
323 *Soc. Rev.* **2017**, *46*, 3322–3356.
- 324 28. Yang, Y.; Tan, B.; Wood, C. Solution-processable Hypercrosslinked Polymers By Low Cost Strategies:
325 a Promising Platform for Gas Storage and Separation. *J. Mater. Chem. A* **2016**, *4*, 15072–15080.
326 doi:10.1039/c6ta05226f.
- 327 29. Dawson, R.; Stöckel, E.; Holst, J.; Adams, D.; Cooper, A. Microporous Organic Polymers for Carbon
328 Dioxide Capture. *Energy Environ. Sci.* **2011**, *4*, 4239–4245. doi:10.1039/c1ee01971f.
- 329 30. Jing, X.; Zou, D.; Cui, P.; Ren, H.; Zhu, G. Facile Synthesis of Cost-effective Porous Aromatic Materials
330 with Enhanced Carbon Dioxide Uptake. *J. Mater. Chem. A* **2013**, *1*, 13926–13931. doi:10.1039/c3ta13115g.
- 331 31. Errahali, M.; Gatti, G.; Tei, L.; Paul, G.; Rolla, G.A.; Canti, L.; Fraccarollo, A.; Cossi, M.; Comotti, A.;
332 Sozzani, P.; Marchese, L. Microporous Hyper-Cross-Linked Aromatic Polymers Designed for Methane
333 and Carbon Dioxide Adsorption. *J. Phys. Chem. C* **2014**, *118*, 28699–28710.
- 334 32. Ratvijitvech, T.; Barrow, M.; Cooper, A.; Adams, D. The Effect of Molecular Weight on the Porosity of
335 Hypercrosslinked Polystyrene. *Polym. Chem.* **2015**, *6*, 7280–7285. doi:10.1039/c5py00668f.
- 336 33. Fu, Z.; Jia, J.; Li, J.; Liu, C. Transforming Waste Expanded Polystyrene Foam Into Hyper-crosslinked
337 Polymers for Carbon Dioxide Capture and Separation. *Chem. Eng. J.* **2017**, *323*, 557–564.
338 doi:10.1016/j.cej.2017.04.090.
- 339 34. Zhang, Y.; Shen, Z.; Yu, Y.; Liu, L.; Wang, G.; Chen, A. Porous Carbon Derived from Waste Polystyrene
340 Foam for Supercapacitor. *J. Mater. Sci.* **2018**, *53*, 12115–12122. doi:10.1007/s10853-018-2513-z.
- 341 35. de Paula, F.; de Castro, M.; Ortega, P.; Blanco, C.; Lavall, R.; Santamaría, R. High Value
342 Activated Carbons from Waste Polystyrene Foams. *Micropor. Mesopor. Mat.* **2018**, *267*, 181–184.
343 doi:10.1016/j.micromeso.2018.03.027.
- 344 36. Zhang, Y.; Qiang, Z.; Vogt, B.D. Relationship Between Crosslinking and Ordering Kinetics for the
345 Fabrication of Soft Templated (FDU-16) Mesoporous Carbon Thin Films. *RSC Adv.* **2014**, *4*, 44858–44867.
346 doi:10.1039/C4RA08316D.

- 347 37. Deng, G.; Zhang, Y.; Ye, C.; Qiang, Z.; Stein, G.E.; Cavicchi, K.A.; Vogt, B.D. Bicontinuous
348 Mesoporous Carbon Thin Films Via An Order-order Transition. *Chem. Commun.* **2014**, *50*, 12684–12687.
349 doi:10.1039/C4CC02471K.
- 350 38. Zhang, C.; Kong, R.; Wang, X.; Xu, Y.; Wang, F.; Ren, W.; Wang, Y.; Su, F.; Jiang, J.X. Porous Carbons
351 Derived from Hypercrosslinked Porous Polymers for Gas Adsorption and Energy Storage. *Carbon* **2017**,
352 *114*, 608–618. doi:10.1016/j.carbon.2016.12.064.
- 353 39. Modak, A.; Bhaumik, A. Porous Carbon Derived Via KOH Activation of a Hypercrosslinked Porous
354 Organic Polymer for Efficient CO₂, CH₄, H₂ Adsorptions and High CO₂/N₂ Selectivity. *J. Solid State*
355 *Chem.* **2015**, *232*, 157–162. doi:10.1016/j.jssc.2015.09.022.
- 356 40. Vinodh, R.; Abidov, A.; Peng, M.; Babu, C.; Palanichamy, M.; Cha, W.; Jang, H.T. Synthesis and
357 Characterization of Semiconducting Porous Carbon for Energy Applications and CO₂ Adsorption. *J.*
358 *Ind. Eng. Chem.* **2015**, *32*, 273–281. doi:10.1016/j.jiec.2015.09.002.
- 359 41. Canti, L.; Fraccarollo, A.; Gatti, G.; Errahali, M.; Marchese, L.; Cossi, M. An Atomistic Model of
360 a Disordered Nanoporous Solid: Interplay Between Monte Carlo Simulations and Gas Adsorption
361 Experiments. *AIP Advances* **2017**, *7*, 045013. doi:10.1063/1.4982069.
- 362 42. Gatti, G.; Olivas Olivera, D.; Sacchetto, V.; Cossi, M.; Braschi, I.; Marchese, L.; Bisio, C. Experimental
363 Determination of the Molar Absorption Coefficient of N-Hexane Adsorbed on High-Silica Zeolites.
364 *ChemPhysChem* **2017**, *18*, 2374–2380. doi:10.1002/cphc.201700481.
- 365 43. Landers, J.; Gor, G.; Neimark, A. Density Functional Theory Methods for Characterization of Porous
366 Materials. *Colloids Surf. A* **2013**, *437*, 3–32.
- 367 44. Thommes, M.; Cychosz, K.A. Physical Adsorption Characterization of Nanoporous Materials: Progress
368 and Challenges. *Adsorption* **2014**, *20*, 233–250.
- 369 45. Zhao, J.; Yang, L.; Li, F.; Yu, R.; Jin, C. Structural Evolution in the Graphitization Process of Activated
370 Carbon By High-pressure Sintering. *Carbon* **2009**, *47*, 744–751. doi:10.1016/j.carbon.2008.11.006.
- 371 46. Cançado, L.; Takai, K.; Enoki, T.; Endo, M.; Kim, Y.; Mizusaki, H.; Speziali, N.; Jorio, A.; Pimenta, M.
372 Measuring the Degree of Stacking Order in Graphite By Raman Spectroscopy. *Carbon* **2008**, *46*, 272–275.
373 doi:10.1016/j.carbon.2007.11.015.
- 374 47. Joseph, R.; Ford, W.T.; Zhang, S.; Tsyurupa, M.P.; Pastukhov, A.V.; Davankov, V.A. Solid-state ¹³C-NMR
375 Analysis of Hypercrosslinked Polystyrene. *J. Polym. Sci. A Polym. Chem.* **1997**, *35*, 695–701.
376 doi:10.1002/(SICI)1099-0518(199703)35:4<695::AID-POLA12>3.0.CO;2-I.
- 377 48. Conte, P.; Carotenuto, G.; Piccolo, A.; Perlo, P.; Nicolais, L. NMR-investigation of the Mechanism
378 of Silver Mercaptide Thermolysis in Amorphous Polystyrene. *J. Mater. Chem.* **2007**, *17*, 201–205.
379 doi:10.1039/B613228F.
- 380 49. Woodward, R.T.; Stevens, L.A.; Dawson, R.; Vijayaraghavan, M.; Hasell, T.; Silverwood, I.P.; Ewing, A.V.;
381 Ratvijitvech, T.; Exley, J.D.; Chong, S.Y.; Blanc, F.; Adams, D.J.; Kazarian, S.G.; Snape, C.E.; Drage, T.C.;
382 Cooper, A.I. Swellable, Water- and Acid-Tolerant Polymer Sponges for Chemoselective Carbon Dioxide
383 Capture. *J. Am. Chem. Soc.* **2014**, *136*, 9028–9035. doi:10.1021/ja5031968.
- 384 50. Wang, Z.; Opembe, N.; Kobayashi, T.; C. Nelson, N.; Slowing, I.; Pruski, M. Quantitative Atomic-scale
385 Structure Characterization of Ordered Mesoporous Carbon Materials By Solid State NMR. *Carbon* **2018**,
386 *131*, 102–110. doi:10.1016/j.carbon.2018.01.087.
- 387 51. Vieira, M.A.; Gonçalves, G.R.; Cipriano, D.F.; Schettino, M.A.; Filho, E.A.S.; Cunha, A.G.; Emmerich,
388 F.G.; Freitas, J.C. Synthesis Of Graphite Oxide from Milled Graphite Studied By Solid-state ¹³C Nuclear
389 Magnetic Resonance. *Carbon* **2016**, *98*, 496 – 503. doi:https://doi.org/10.1016/j.carbon.2015.11.037.
- 390 52. Parvez, K.; Wu, Z.S.; Li, R.; Liu, X.; Graf, R.; Feng, X.; Müllen, K. Exfoliation of Graphite Into Graphene
391 in Aqueous Solutions of Inorganic Salts. *J. Am. Chem. Soc.* **2014**, *136*, 6083–6091. doi:10.1021/ja5017156.
- 392 53. Cai, W.; Piner, R.D.; Stadermann, F.J.; Park, S.; Shaibat, M.A.; Ishii, Y.; Yang, D.; Velamakanni, A.; An, S.J.;
393 Stoller, M.; An, J.; Chen, D.; Ruoff, R.S. Synthesis and Solid-State NMR Structural Characterization of
394 ¹³C-Labeled Graphite Oxide. *Science* **2008**, *321*, 1815–1817. doi:10.1126/science.1162369.
- 395 54. Gao, W.; Alemany, L.; Ci, L.; Ajayan, P. New Insights Into the Structure and Reduction of Graphite Oxide.
396 *Nat. Chem.* **2009**, *1*, 403–408. doi:10.1038/nchem.281.
- 397 55. Huang, P.; Schwegler, E.; Galli, G. Water Confined in Carbon Nanotubes: Magnetic Response and Proton
398 Chemical Shieldings. *J. Phys. Chem. C* **2009**, *113*, 8696–8700. doi:10.1021/jp811060y.

- 399 56. Kibalchenko, M.; Payne, M.C.; Yates, J.R. Magnetic Response of Single-Walled Carbon Nanotubes
400 Induced By An External Magnetic Field. *ACS Nano* **2011**, *5*, 537–545. doi:10.1021/nn102590b.
- 401 57. Forse, A.C.; Griffin, J.M.; Presser, V.; Gogotsi, Y.; Grey, C.P. Ring Current Effects: Factors Affecting the
402 NMR Chemical Shift of Molecules Adsorbed on Porous Carbons. *J. Phys. Chem. C* **2014**, *118*, 7508–7514.
403 doi:10.1021/jp502387x.
- 404 58. Nguyen, H.; Espinal, L.; van Zee, R.; Thommes, M.; Toman, B.; Hudson, M.; Mangano, E.; Brandani, S.;
405 Broom, D.; Benham, M.; Cychosz, K.; Bertier, P.; Yang, F.; Krooss, B.; Siegelman, R.; Hakuman, M.; Nakai,
406 K.; Ebner, A.; Erden, L.; Ritter, J.; Moran, A.; Talu, O.; Huang, Y.; Walton, K.; Billefont, P.; De Weireld,
407 G. A Reference High-pressure CO₂ Adsorption Isotherm for Ammonium ZSM-5 Zeolite:
408 Results of An Interlaboratory Study. *Adsorption* **2018**, *24*, 531–539. doi:10.1007/s10450-018-9958-x.
- 409 59. Li, Y.; Ben, T.; Zhang, B.; Fu, Y.; Qiu, S. Ultrahigh Gas Storage Both At Low and High Pressures in
410 KOH-activated Carbonized Porous Aromatic Frameworks. *Sci. Rep.* **2013**, *3*. doi:10.1038/srep02420.
- 411 60. Hilton, R.; Bick, P.; Tekeei, A.; Leimkuehler, E.; Pfeifer, P.; Suppes, G. Mass Balance and Performance
412 Analysis of Potassium Hydroxide Activated Carbon. *Ind. Eng. Chem. Res.* **2012**, *51*, 9129–9135.
413 doi:10.1021/ie301293t.

414 © 2019 by the authors. Submitted to *Nanomaterials* for possible open access publication
415 under the terms and conditions of the Creative Commons Attribution (CC BY) license
416 (<http://creativecommons.org/licenses/by/4.0/>).